Bioprinting 16 (2019) e00058

Contents lists available at ScienceDirect

Bioprinting

journal homepage: www.elsevier.com/locate/bprint

A mechanically robust thixotropic collagen and hyaluronic acid bioink supplemented with gelatin nanoparticles

Casey C. Clark [a,b], Julio Aleman [a], Lysette Mutkus [a], Aleksander Skardal [a,b,c,d,e,1,2,*]

[a] Wake Forest Institute for Regenerative Medicine, Wake Forest School of Medicine, 391 Technology Way, Winston-Salem, NC, 27101, United States
[b] Virginia Tech-Wake Forest School of Biomedical Engineering and Sciences, Wake Forest School of Medicine, Medical Center Boulevard, Winston-Salem, NC, 27157, United States
[c] Department of Cancer Biology, Wake Forest School of Medicine, Medical Center Boulevard, Winston-Salem, NC, 27157, United States
[d] Department of Molecular Medicine and Translational Science, Wake Forest School of Medicine, Medical Center Boulevard, Winston-Salem, NC, 27157, United States
[e] Comprehensive Cancer Center at Wake Forest Baptist Medical, Medical Center Boulevard, Winston-Salem, NC, 27157, United States

ARTICLE INFO

Keywords:
Bioprinting
Materials science
Bioink

ABSTRACT

Bioprinting has become an essential tool of biomedical engineering and regenerative medicine. However, current biologically relevant bioinks, i.e. printing materials made from materials found within the extracellular matrix, are unable to support themselves and require a sacrificial support material to create large structures. To address this issue, we have developed a novel thixotropic bioink made from methacrylated collagen I, thiolated hyaluronic acid, and gelatin nanoparticles which is self-supporting and capable of creating large hollow structures through bioprinting. Once printed, this material can be photo-crosslinked to finalize the structure and can be immerse in media for culture with minimal swelling. An intersecting tubular structure 5 mm in diameter with a 1 mm wall thickness was able to be printed longitudinally without support material using a CellInk BIOX bioprinter. This bioink was also able to support HepG2 cells in bioprinted organoids, with adenosine triphosphate assays and immunohistochemistry showing proliferation. Responses to acetaminophen and troglitazone were as expected, proving that the new bioink does not significantly alter HepG2 drug response. With great mechanical properties as well as good biocompatibility, this new biologically relevant bioink is a great improvement over current bioinks.

1. Introduction

Bioprinting has become a staple technology of regenerative medicine and tissue engineering, with extrusion bioprinting being the most common printing modality [1–3]. It allows for 3D tissue constructs to be fabricated on demand in a variety of shapes and sizes with multiple combinations of cells by extruding cellularized hydrogels, or "bioinks", out of syringes, which can be fit with nozzles of different diameters, to create cellularized constructs. These living constructs can be used for 1) therapeutic applications, or 2) novel *in vitro* models of tissues that more accurately represent the *in vivo* pathology [3,4]. While this technology is a useful tool for biomedical applications, the materials that are currently in use for bioprinting limit the overall potential of bioprinting.

The major limitation of these extrusion bioinks is the balance between biocompatibility and printability [4,5]. One common solution is to use multiple printheads to print multiple materials in one print – one that is biocompatible and one that is mechanically stable. This is similar to conventional 3D printing, where a model material is used in tandem with a sacrificial support material to create complex structures. The biocompatible "model" bioink will be printed with cells embedded and it will eventually turn into the living tissue. The other "support" material does not have any cells but provides a mechanically stable structure for the cellularized bioink to adhere to. The support material is, at the very least, bio-inert and has to be removed once the entire print is finished. This dual model/support system is seen across the field to increase model complexity without improving the model material [6–18]. The model materials needing support are commonly low concentration bioinks, around 10 mg/mL, and are typically hydrogels like gelatin methacrylate (GelMA), collagen, alginate, fibrin, solubilized ECM, and polyethylene glycol [6–18]. The support material can also be added to the model material so that only one material needs to be printed [19,20]. However, the support material is rarely incorporated in the final construct, and if it is not biologically relevant to mammalian tissue, like pluronic F-127,

* Corresponding author. Tzagournis Medical Research Facility, Suite 514A, 420 W 12th Ave, Columbus, OH, 43210, United States.
E-mail address: skardal.1@osu.edu (A. Skardal).
[1] Department of Biomedical Engineering, The Ohio State University, Bevis Hall, 1080 Carmack Drive, Columbus, OH, 43210 (current affiliation).
[2] The Ohio State University Comprehensive Cancer Center, 460 W 10th Ave, Columbus, OH 43210 (current affiliation).

https://doi.org/10.1016/j.bprint.2019.e00058
Received 24 April 2019; Received in revised form 11 July 2019; Accepted 6 August 2019
2405-8866/© 2019 Published by Elsevier B.V.

Relevant abbreviations:

HA	hyaluronic acid
TRO	Troglitazone
GNP	Gelatin nanoparticles
DPBS	Dulbecco's modified phosphate buffered saline
ColMA	collagen methacrylate
APAP	Acetaminophen
ζ°	zeta potential
G′	Storage modulus
G″	Loss Modulus
DLS	Dynamic Light Scattering
SEM	Scanning Electron microscope/microscopy
DI	Deionized
γ	Shear Strain

cellulose nanofibers, and polycaprolactone, it will need to be degraded and replaced before the bioprinted construct can be implanted. Thus, the need for a mechanically stable and biocompatible bioink made from biologically-derived materials found in mammalian extra cellular matrix (ECM) is still an outstanding advancement in bioprinting that requires addressing.

The ideal bioink would one that is self-supportive, biologically relevant, cell-interactive, and protects the cells from the printing process. The self-supporting property would allow for increased precision, increased model complexity, greater aspect ratio structures, and decreased maturation time. The latter meaning that complex models can be accurately made without a support material allowing for the bioprinted construct to mature sooner. Being biologically relevant and recognizable to cells allows the cells to behave appropriately with a higher viability. Cellular function is dependent on their chemical and mechanical environment, so biologically relevant materials are needed to provide the proper mechanical and chemical signals similar to those the cells would experience *in vivo* [21–26]. Optimally, the materials from which the bioink is formulated would be derived from components that contribute to the native tissue extracellular matrix, such as collagen, hyaluronic acid, chondroitin sulfate, and adhesion proteins [27–29]. Protection from the printing process is necessary because the processing method can be violent, relatively speaking, with high pressures and shear forces which can decrease cellular viability [30–32]. A material that can protect the cells from such detrimental variables, by 1) providing insulation from the pressure and 2) being shear thinning to alleviate exposure to shear stresses during printing, would serve to improve cell viability once printed.

These mechanical properties, when taken together, describe a thixotropic material. Thixotropy is a special case of shear thinning where the material will behave as a solid under low shear conditions, but then quickly transition into a liquid once a critical shear strain is reached [33]. Examples of thixotropic materials are mayonnaise, toothpaste, and wet sand. All of these can hold their shape and be solid, but can still be molded, and will flow if enough shear/pressure is applied. There exist several thixotropic bioinks already, such as cellulose nanofibers and pluronic F-127, but these are not representative of native ECM and will not be recognized by cells. A thixotropic bioink made entirely of ECM-derived materials would be the ideal bioink for extrusion bioprinting.

Herein we describe a novel bioink that is comprised entirely of materials found within human tissue ECM that has excellent mechanical properties and printability. This was achieved by incorporating gelatin nanoparticles (GNPs) into a base bioink made from methacrylated collagen (ColMA) and a heparin-conjugated and thiolated hyaluronic acid (HA) [34]. The GNPs induce thixotropy by the physical and, to a lesser degree, intermolecular interactions they provide within the bioink. This bioink is extensively characterized mechanically and employed in a variety of demonstrations of printability to show its superior characteristics to the base bioink. Lastly, biocompatibility is confirmed through deploying the bioink, with cells incorporated, in several viability assays. Bioprinting technology holds immense potential in a variety of biomedical applications, yet bioink development has typically lagged behind the development of printer hardware. Advances in bioink materials, such as that described here, aim to provide cell-friendly and robust printability for these future applications.

2. Materials and methods

2.1. Base bioink formulation

The base bioink composition is made from methacrylated collagen (Advanced BioMatrix, Carlsbad, CA, Catalog #5201-1KIT), initially dissolved in sterile filtered 20 mM acetic acid solution (Advanced BioMatrix) at 6 mg/mL. This solution was kept refrigerated at 4 °C until needed. When ready for use, aliquots were removed and neutralized with a neutralization solution (Advanced BioMatrix) made of sodium hydroxide in phosphate buffered saline (pH 10.5), which was sterile filtered before use, according to the manufacturer's protocol: 85 μL per mL of 6 mg/mL methacrylated collagen dissolved in the 20 mM acetic acid solution. Thiolated HA (Heprasil, ESI BIO, Alameda, CA) was dissolved at 10 mg/mL with deionized (DI) water provided from an in-house supply with 1 mg/mL of Irgacure 2959 (Sigma-Aldrich, St. Louis, MO), added as the photoinitiator for UV crosslinking. The ColMa and HA solutions were then mixed in a 3:1 ratio by volume prior to use.

2.2. Gelatin nanoparticle preparation

Gelatin nanoparticles (GNPs) were made using a process based on the two-step desolvation method originally developed by Coester et al. [35]. Briefly, 2.5 g gelatin type B, 255 bloom (Sigma-Aldrich, St. Louis, MO) was dissolved in 50 mL DI water at 40 °C with vigorous stirring. Then, 50 mL acetone (Sigma-Aldrich) was added. The solution was removed from the stir plate and left to sit at room temperature for 1 h to allow high molecular weight gelatin to precipitate. After the hour, the supernatant was decanted, and the remaining precipitated gelatin was redissolved in 50 mL DI water at 40 °C with vigorous stirring. The pH was adjusted to 2.5 using 12 M HCl and 10 M NaOH (Fischer Scientific, Hampton, NH). 150 mL of acetone was then added at a rate of approximately 5 mL/min. Once added, 200 μL of 25 %V/V glutaraldehyde in water (Sigma-Aldrich) was then added to the solution. The solution was gently stirred overnight at 40 °C to complete the reaction. The pH of the solution was then neutralized with 10 M NaOH which aggregated and precipitated the GNPs. These were then collected, redispersed in 200 mL Dulbecco's phosphate buffered saline (DPBS) (Thermo Fisher Scientific, Waltham, MA) to wash them of impurities. The solution was then centrifuged at 4600 RCF for 5 min to collect the GNPs in a pellet. The redispersion in PBS and centrifugation process was performed two more times to wash the GNPs of any impurities. The final pellet was collected by redispersing it in a small amount of DI water. This pellet was then frozen overnight at -20 °C, and then lyophilized for 3–5 days until completely dry. The resulting solid was then pulverized by hand with mortar and pestle and then cryomilled to powder the solid. The resulting powder was stored at room temperature in a water tight glass scintillation vial until further use.

2.3. GNP analysis

Scanning electron microscopy (SEM) analysis was performed on a FlexSEM1000 (Hitachi, Schaumburg, IL) at 15 kV. The samples were prepared by placing some of the lyophilized GNPs on carbon tape, and then sputter coating the material with gold and palladium. The GNPs were also analyzed using dynamic light scattering (DLS) for size distribution and zeta potential (ζ°) for aqueous stability using a Malvern

Panalytical Zetasizer Nano Range (Malvern Panalytical, Malvern, United Kingdom). For each, the GNPs were added to the appropriate polystyrene cuvette immediately after synthesis, or after being dispersed in DI water after the cryomilling procedure, and then the analysis was performed. The GNP powder before and after cryomilling was observed under a Leica DMi1 (Leica Microsystems, Buffalo Grove, IL) microscope to compare their morphologies.

2.4. GNP bioink preparation

The GNP powder was sterilized by dry heating the powder at 100 °C for 30 min. They were then added, at 100 mg/mL, 125 mg/mL and 150 mg/mL, to the ColMA while it was still in acetic acid solution. This was mechanically stirred in to create a thick paste. This addition was performed at least two days prior to use, stirring frequently to completely hydrate and disperse the GNPs in the hydrogel. When ready to use, the ColMa and GNP material was neutralized as described above, and then the thiolated HA solution, prepared as described above, was added at the proper ratio. All concentrations of GNPs in the hydrogel bioink are reported as their final concentration in the complete hydrogel volume. The material was kept refrigerated at all times to prevent the collagen from forming fibers and to slow the spontaneous bonding of methacrylate groups with thiol groups.

2.5. GNP bioink mechanical analysis

Once all components of the bioink were mixed, the bioink was analyzed using a TA instruments DHR-2 rheometer (TA Instruments, New Castle, DE) with a 25 mm plate and 25 mm 2 ° cone system with 120 grit sandpaper intimately bonded to the surfaces. This addition mimics a roughened geometry for better adhesion to the bioink, preventing slippage during testing. Three analyses were performed: a strain sweep from 1 % to 1000 % shear strain (γ), a thixotropic analysis where alternating low strain (10 %γ) and high strain (500 %γ) was applied, and then a thixotropic recovery analysis where a strain pattern of low-high-low was performed. The strain sweep was performed to determine overall stiffness and elasticity of the bioinks along with the critical shear strain to induce a liquid transformation. The thixotropic analysis was performed to understand the reversible and repeatable behavior of the thixotropic mechanism. The thixotropic recovery analysis was performed to determine how much time was required for the bioink to regain all of its initial mechanics. The strain sweep was also performed on UV crosslinked GNP bioink samples to determine their mechanical properties once crosslinked. The samples were crosslinked by exposure to 365 nm UV light at 1.39 W/cm^2 for 10 s.

2.6. GNP bioink printing

The non-cellularized bioink underwent print testing using a CellInk Inkredible pneumatic bioprinter and a CellInk Bio X bioprinter with a syringe pump printhead (CellInk, Gothenburg, Sweden). All model prints were performed with a 3 mL BD Falcon syringe (Fischer Scientific) with a ½" 22 Ga blunt needle (CellInk, Gothenburg, Sweden) as the print nozzle, a print speed of 10 mm/s, a layer height of 0.2 mm, with single perimeter printing, no infill, and no supporting material. The pneumatic print head had pressure set around 250 kPa, adjusting for the heterogeneities in the bioink as they appeared during the print, while the syringe pump head was set to extrude at 0.75 μL/mm of printing. All printed constructs were UV crosslinked using 365 nm light at an intensity of 1.39 W/cm^2 after printing. All 3D model architectures were developed in AutoDesk Inventor and sliced with Slic3r, or CellInk's onboard slicing software depending on the printer used.

2.7. GNP bioink swelling

Non-cellularized bioink was placed into a 8 mm × 0.5 mm silicone mold and cured with UV light for 10 s. The disks were then removed, weighed, placed into 150 mm culture dish with 20 mm grid (Corning, Corning, NY), and submerged in PBS. Top-down pictures were taken of the disks and the grid was used as a scale for image analysis using GNU Image Manipulation Program (GIMP) image manipulation software to determine diameter. The next day, the disks were again measured and weighed for comparison to their starting values.

2.8. Organoid immersion printing

Gelatin was sterilized by dry heating the material to 100 °C for 30 min, after which it was then dissolved at 40 °C in a sterile filtered solution of 1 mg/mL Irgacure 2959 dissolved in DI water, to reach a gelatin concentration of at 10 mg/mL. One mL of gelatin solution was then deposited into each well of a non-tissue culture treated Corning Falcon 48-well plate (Fischer Scientific). The plate was then placed in the refrigerator to cool overnight before bioprinting. When ready to print, the plate was placed in the Inkredible printer's print stage, which was then homed and calibrated, and then a specifically designed and sliced CAD file was created that instructed the printer to place one organoid per well. Each organoid was approximately 20 μL in volume. The print head nozzle was calibrated to a depth such that all extrusion would take place within the gelatin bath. All organoid printing was performed with the Inkredible in a 4 °C cold room to prevent the collagen component of the bioink from setting up as previously described. Once printed, the plate was exposed to UV light (365 nm at an intensity of 1.39 W/cm^2) for 10 s to permanently crosslink the organoids. Several plates of organoids were produced this way so that malformed organoids could be discarded, while still maintaining enough organoids for all subsequent studies.

2.9. Cell culture

HepG2 cells (American Type Culture Collection, Manassas, VA) were cultured using a media made of high glucose Dulbecco's modified eagle medium (DMEM, Fischer Scientific) supplemented with 10% fetal bovine serum (Sigma-Aldrich), 1% penicillin and streptomycin solution (Fischer Scientific), and 1% L-glutamine solution (Fischer Scientific). Cells were incubated at 37 °C at 5 % CO_2 and 95% humidity in Panasonic incubators (PHC Corporation of America, Wood Dale, IL). Cells were seeded into 150 mm Corning Falcon tissue culture plates (Fischer Scientific, Hampton, NH) at 2 million cells per plates, with 15 mL of media, and allowed to grow until confluent, swapping media every 2 days. Cell cultures were split by removing the media, washing twice with 2 mL DPBS, adding 7 mL of TrypLE solution (Thermo Fisher Scientific), and incubating for 5 min or until the cells were completely detached with gentle agitation. The TrypLE solution was then neutralized with 7 mL of culture media. The cell suspension was then collected and spun down in the previously mentioned centrifuge at 1100 RCF for 5 min. The supernatant was then discarded, and the cells were redispersed in 5 mL of media for counting. Cells were counted using a Nucleo View 200 automated cell counter (Cemometec, Allerod, Denmark). Cells were then reseeded at the previously described conditions for further culture.

2.10. Proliferation study

Organoids were prepared as described previously with HepG2 cells at a cell density of 5 million per mL of bioink. The cells were first added to the thiolated HA, which was then mixed into the other bioink components as previously described. This cellular bioink was then loaded into pneumatically driven syringes (CellInk) as previously described for the organoid immersion printing method. Once printed and crosslinked, the plates were placed in the incubator until the gelatin immersion material was melted, about 15 min. The gelatin was then removed, and the each well was filled with 500 μL of media. The media was swapped every other day for the duration of the study. Before the media is added, the organoids undergo visual inspection to make sure none are too large

(specifically, greater than 40 μL volume), organoids were fully cross-linked, and consistent in shape. Oversized, soft, or fragmented organoids created a variety of problems during culture and analysis and were thus discarded before the experiment started. Six organoids were selected at random on days 1, 3, 5, 7, 9, 11, and 13, and moved to a sterile Corning Falcon non tissue culture treated 48-well plate (Fischer Scientific) for analysis. These organoids had their media aspirated and replaced with 100 μL of room temperature media and 100 μL of room temperature Cell Titer Glo 3D ATP assay solution (Promega, Madison, WI). The plate was then shaken on a vortex (Fischer Scientific) at low speed (200 RPM) for 10 min, and then allowed to rest at room temperature for an additional 20 min 150 μL of the solution was then transferred to a white opaque 96-well plate and luminescence was quantified on a Varioskan Lux multimode microplate reader (Thermo Fisher, Waltham, MA). Each organoid was then weighed using a Mettler-Toledo microbalance (Mettler-Toledo, Columbus, OH). The recorded ATP signal was then divided by the organoid mass to normalize the signal to account for any remaining variance in organoid size.

2.11. Drug study

Organoids were prepared as previously described and maintained in culture for 7 days. At this point, the media was swapped for fresh media containing acetaminophen (APAP, Sigma-Aldrich) at 100 μM, 1 mM, and 10 mM; and troglitazone (TRO, Sigma-Aldrich) at 10 μM, 100 μM and 1 mM. The drug-containing media was prepared by first dissolving the drug in DMSO (Sigma-Aldrich), and then preparing serial dilutions to produce the lower concentrations. The maximum DMSO concentration was 1 %v/v, and so a control was added which was media supplemented with 1 % DMSO. Another control, which was media with no supplement, was also employed in tandem. Each condition was performed in triplicate. The organoids were cultured for 2 days with their respective conditions, after which the organoids were subjected to the same ATP assay described previously, and mass normalized.

2.12. Immunohistochemistry

Organoids at day 1, 7, and 13, of the growth study were collected and prepared for IHC using three organoids per time point. The organoids were removed from culture, washed with DPBS, and then placed in 4 % formaldehyde (PFA), prepared from a 32% stock solution purchased (Sigma-Aldrich), and gently shaken overnight at 4 °C. The organoids were then removed from the PFA solution and placed in a 70 % ethanol solution, made from 100% stock solution (Warner-Graham, Cockeysville, MD), and left at 4 °C for storage. The organoids were removed from ethanol and embedded in paraffin. Sections of 4 μm thickness were cut from paraffin embedded HepG2 GNP bioink organoids with a microtome and placed on glass slides. The slides were deparaffinized in xylene, rehydrated, and washed three times in water. They were then permeabilized using 0.2% Triton-X100 in PBS, followed by three tris buffered saline (TBS, Sigma-Aldrich) washes, after which they underwent antigen retrieval. The slides were submerged in pH 6.0 AR Citrate buffer (PerkinElmer, Waltham, MA) in a bead bath at 95 °C for 20 min, washed three times with TBS, and then blocked using protein block (Dako, cat# X0909) for 10 min at room temperature. Organoids were stained using an Opal color kit (PerkinElmer, cat# NEL797001KT). Primary antibodies (Ki67, 1:100 dilution, abcam cat# ab16667) diluted in antibody diluent (Dako, Agilent, Santa Clara, CA, cat # S3022) were applied over the course of 2 consecutive days overnight at 4 °C following each with an accompanying HRP 2^{o} (anti-rabbit) for 30 min at room temperature, and then Opal fluorophore 570 & 540 diluted in amplification diluent at room temperature for 10 min. Slides were then washed three times with TBS supplemented with 0.5 % TWEEN 20 (Sigma-Aldrich) , and then stained with DAPI (1:10,000 dilution in PBS), followed by three TBS washes, mounted with Prolong glass (Invitrogen, Calsbad, CA, cat# P36984), cover slipped, and imaged using an Olympus BX63 microscope (Olympus, Center Valley, PA).

3. Results and discussion

3.1. Nanoparticle analysis

The nanoparticles produced were roughly 300 nm in diameter immediately after synthesis as estimated from SEM micrographs, shown in Supplemental Fig. 1A. This was corroborated by the DLS analysis, showing that immediately following synthesis, the GNPs are roughly 400 nm in diameter (Supplemental Fig. 1B), very similar to the estimation from the SEM micrograph. This is likely due to swelling from being immersed in water. These GNPs are also moderately stable in aqueous suspension with a ζ° of nearly +20 mV (Supplemental Fig. 1C). This stability is necessary for the GNPs to remain in a homogeneous suspension in the bioink.

The purification and cryomilling processes needed to produce a powder that is able to be easily incorporated into the bioink has some effect on GNP morphology. During the purification process, the GNPs aggregate and fall out of solution. Supplemental Fig. 2 shows the comparison between the synthesis solution before and after neutralization, which causes large aggregates to form. This aggregation creates physically entangled GNPs that are unable to be mechanically separated. The cryomilling procedure dramatically reduces the size of the collected mass to aggregates that are 5 μm in diameter (Supplemental Fig. 1D). This DLS analysis was corroborated by light microscopy between the two powders (Supplemental Fig. 3). The morphology of the individual GNPs has not changed, though they are introduced into the bioink now in aggregate form rather than as individual nanoparticles. These aggregates slowly break apart once redispersed into the bioink which will be shown later in the IHC analysis of the organoids. Once redispersed, the new ζ° is -20mV, again indicating that moderate aqueous stability is achieved (Supplemental Fig. 1E).

It may not be critical that individual GNPs are present in the bioink to induce the proper mechanics. As long as the particles are small enough to have significant physical interactions, like capillary action pulling two nearby particles together, as well as significant intermolecular interactions, like collagen fibers intermolecularly bonding to the GNP surfaces, then a mechanically stable bioink should still be produced.

3.2. Bioink mechanics

Rheological analysis of the GNP bioink confirms that a robust, self-supporting, thixotropic bioink has been produced with the cryomilled GNPs. The rheological profiles of the bioink with various amounts of cryomilled GNPs is shown in Fig. 1A below, along with the base bioink's mechanics, and non-cryomilled GNP bioink's mechanics, for comparison. Supplemental Tables 1 and 2 list some of the important mechanical values to compare between the tested bioinks. The GNP bioink profiles can be broken up into three different regimes: solid, transition, and liquid. The solid regime is present at low strains, typically below 50% shear strain. This is where the bioink behaves as a solid with a plateau in mechanics due to the physical and molecular interactions provided by GNPs. In this regime, the shear elastic modulus, $\boldsymbol{G'}$, is typically greater numerically than the shear loss modulus, $\boldsymbol{G''}$. The transition regime is present during moderate shearing, generally from 50% to 200% shear strain. During this period, the bioink's internal physical and molecular interaction begin to break down and the bioink transitions into a liquid. In this regime, the magnitudes of $\boldsymbol{G'}$ and $\boldsymbol{G''}$ converge. The liquid regime is present at high strain, typically greater than 200% shear strain, where $\boldsymbol{G''}$ is greater than $\boldsymbol{G'}$. The strain at which the material transitions from a solid to a liquid is the thixotropic point. All of these regimes' shear strain values will shift up or down if more or fewer GNPs are present in the bioink because the amount of internal interactions present will also be going up or down proportionally. Here, the transition strains are 237% ± 3.7%, 296% ± 2.01%, and 290% ± 2.31% for the 100 mg/mL,

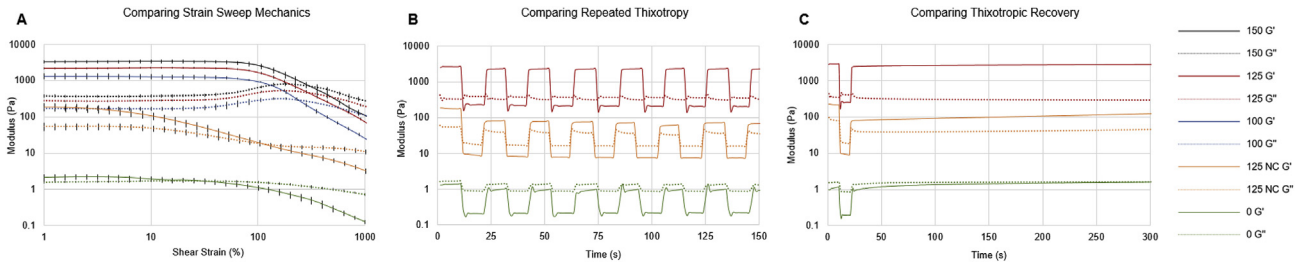

Fig. 1. A) Strain sweep of various bioinks, B) Multiple low/high shear events showing the reversible nature of the bioinks, **C)** One high shear event showing the recovery rate of the bioinks. Legend number refers to GNP concentration in mg/mL, NC denotes non-cryomilled GNPs, error bars are ±1 standard deviation.

125 mg/mL, and 150 mg/mL GNP bioinks, respectively. These mechanics are similar to the post-crosslinked mechanics, as seen in Supplemental Fig. 3. This confirms that in the final state of the bioink, the construct will have similar stiffness to some native tissue, around 1 kPa G′, which will ensure a similar mechanical environment to natural ECM. From this collected data and printing experiments (discussed below), the 125 mg/mL bioink was selected as the standard bioink and was used in all subsequent experiments.

This transition from solid to liquid behavior based on the amount of shear present in the biomaterial is a critical feature for bioprinting. The initial solid regime proves that under normal resting conditions, the bioink will be able to withstand a load applied to it, meaning that it will not deform under its own weight or extra weight applied from above. This makes it a robust bioink that can be used to create hollow structures without any sacrificial support materials, such as pluronic F127 or cellulose nanofibers. The transition to a liquid due to high shear is needed for the bioink to be extrudable and to protect the cells. A very solid material would not extrude well and would require exceedingly high stresses to extrude. These high stresses could potentially rupture cells encapsulated within. This transition also allows for the bioink to flow under the high strain conditions, relieving internal stresses encountered within a bioprinter's nozzle, and then quickly transitioning back to a solid once deposited. This reversible strain dependent behavior can be seen in Fig. 1B and C on the right. Fig. 1B shows how the bioink can cycle between low and high strain, and consequently cycle between solid and liquid, repeatedly without a significant loss in overall mechanics. The test itself is destructive, and so the bioink does not immediately fully recover its original mechanics during the low strain period before the next high strain period. Fig. 1C shows that over several minutes time the bioink will fully recover to its initial mechanics. Extrapolating this linear recovery in G′, it is estimated that the bioink will take approximately 7 min to fully recover its solid regime mechanics, however, >75% of the bioink's original mechanics are restored within 1 s of high strain removal. This shows that as soon as the bioink exits the extrusion nozzle it will setup as a largely solid hydrogel again to preserve the printed geometry.

As mentioned previously in section 3.1, and as will be discussed in section 3.4, the GNPs were not fully dispersed, and following the mechanical analysis of the bioink it is confirmed that full dispersion is not needed for the GNPs to induce the targeted mechanics. However, to achieve these mechanics, the aggregates must be of small enough size where those interactions becomes significant forces. Comparing the cryomilled GNP aggregates, which are 5 μm in diameter, to the non-cryomilled GNP aggregates, which are about an order of magnitude larger with varying sizes, the non-cryomilled aggregates do not achieve the proper mechanics. Supplemental Fig. 4 shows the size comparison between the two powders, and Fig. 1 also shows the rheological and thixotropic profiles of the GNP bioink made with non-cryomilled GNPs. The cryomilled particles are the right size to physically and intermolecularly interacting with each other and the dissolved biomaterials as was described in section 1. The non-cryomilled particles are too large for those interactions to have a significant effect on mechanical behavior, and thus do not produce as robust of a material. This suggests a correlation between GNP size and mechanics, though this relationship was not studied. All of the bioinks with GNP additions show significant improvement over the base bioink.

The physical interactions come in two forms: particle-particle and particle-fiber. The particle-particle interactions occur when two GNPs, or GNP aggregates, come close enough together in the hydrogel carrier solution such that capillary action is induced. This type of particle-particle interaction is also seen in sand castles, where the water shells surround the grains of sand interact with each other and the capillary action between those particles holds them together. The particle-fiber interactions come from the GNP aggregates interacting with the collagen fibers. These fibers will form spontaneously when the collagen is at a neutral pH and around room temperature. These soft fibers will entangle the GNP aggregates to create a network of solid particles held together in a web of collagen. The intermolecular interactions come from the individual molecular chains of collagen and hyaluronic acid interacting with the GNPs and aggregates. There are hydrophilic and hydrophobic sections of the GNPs and collagen chains that will self-assemble, as well as Van der Waals forces and hydrogen bonding between the GNPs, collagen, and hyaluronic acid. These intermolecular forces will the dominant force on the individual GNPs while the physical interactions will be dominant on the micron sized GNP aggregates due to their greater size. These internal forces governing the mechanics are described visually in Fig. 2.

3.3. Bioink printing

From a quantitative standpoint, the mechanical analysis determined that the bioink should switch to a liquid regime when being forced through the printing nozzle, and quickly regain its solid regime mechanics post extrusion, making it a much improved printing material. The qualitative analysis of printing a model confirmed this prediction as well. Fig. 3 compares a CAD model rendition (Fig. 3A–D) to the printed part using this novel bioink (Fig. 3E–L). The structure was chosen to model intersecting vessels, something that modern bioprinters can not produce without support materials or non-biological materials.

This print was performed at room temperature without any support material and the completed hollow structures remained free standing, with only some malformations due to heterogeneity within the bioink (Fig. 3E and H). Using a syringe pump print head that is controlled volumetrically, rather than a pneumatic print head, compensates for most of the heterogeneities of the bioink. However, when thicker regions of the bioink would pass through the nozzle, the printhead piece that connects to the syringe plunger deflects under the high load needed to extrude the material. This deflection causes potential energy to build up, like a spring, which is then released once the thicker portion of the bioink is through the nozzle, causing the print head to extrude more material than the target extrusion rate intends to extrude. These issues produced prints that were close to the original CAD model, with many areas being thicker than modeled due to over-extrusion. For comparison, the CAD model wall thickness was 0.5 mm while the printed model wall thickness averaged about 2 mm. Even with these issues, this novel bioink is

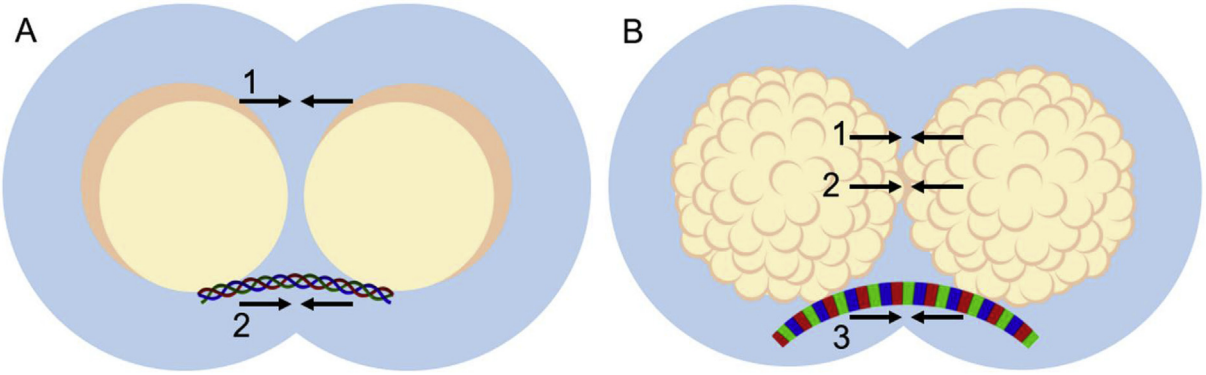

Fig. 2. A) GNP-GNP interactions comprised of 1) electrostatic, capillary, and intermolecular forces and 2) collagen helix binding. B) Aggregate-aggregate interactions comprised of 1) capillary forces, 2) physical entanglement and 3) collagen fibril binding.

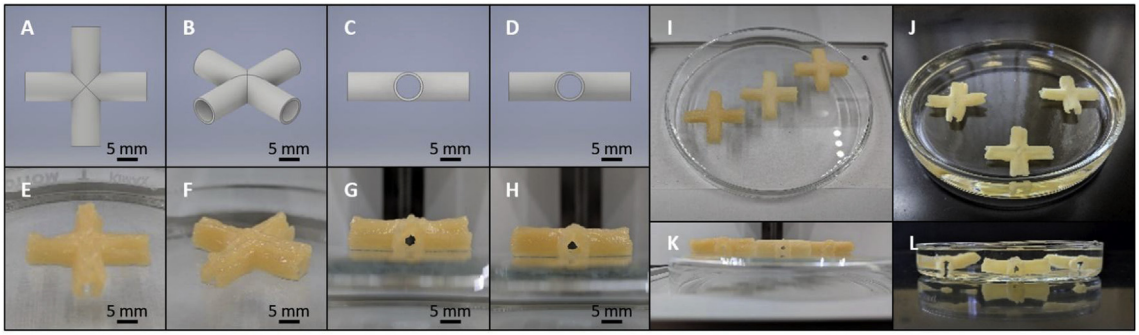

Fig. 3. A) Top, B) orthogonal, C) front, and D) side views of the CAD model. A) Top, B) orthogonal, C) front, and D) side views of the printed model. Top view of three models arranged on a I) glass dish and J) submerged in PBS, with their respective side views K) and L).

printable, and can withstand several layers built up without falling in on itself, eliminating the need for any additional support materials. Furthermore, this printing procedure is reproducible, creating very similar constructs in quick succession (Fig. 3I and K). Precision could be improved by improving the stiffness of the syringe pump hardware by fabricating it with more robust materials. This will decrease any deflection and improve extrusion consistency. Removing all air bubbles and heterogeneities from the material would also reduce the ability for potential energy buildup, though this is difficult since the material is thick and requires vigorous mixing.

Once UV crosslinked following printing, the completed structures are strong enough to be removed from the print surface and manipulated by hand. These structures remain intact once submerged with only minimal swelling. Swelling studies indicate that this bioink swells, on average, 25 ± 5 %m/m and 3.0 ± 5 %l/l (Supplemental Tables 1 and 2). In Fig. 3J and L the models are submerged in DPBS to approximate the swelling that would be seen during culture conditions. The swelling caused some areas along the bottom of the prints to rupture. This part of the print is the thinnest section since layer heights are typically smaller for the first layers and because the bioink is just beginning to extrude during this time. This can be mitigated by including a raft or nozzle priming in the slicing software. The raft would increase the thickness of model bottom, and the nozzle priming would ensure that the material is ready to flow out of the nozzle immediately following pump start up. This was the only region of the prints that showed any signs of damage. This proves that the large quantity of GNPs does not affect UV crosslinking, and that prints are reproducible and will remain solid during culture.

3.4. Biocompatibility

Results from the proliferation study confirm that this new bioink is capable of supporting HepG2 cells and their proliferation (Fig. 4A). An increase in ATP signal is initially seen, corresponding to cell proliferation, and then a plateau occurs with increased variance. Comparing these results to the IHC results (Fig. 4C – E), this increase in variance comes from the directional proliferation and death of the cells. Fig. 4I shows large amounts of cells at the surface of the organoid at day 13, compared to the original dispersion of the cells seen in Fig. 4C at day 1. This can be attributed to the size of the organoids, about 20 μL which will be discussed later, and poor diffusion through this bioink. This new bioink is very thick, as described in section 3.2, which means that diffusion is going to be slower than typical bioinks and the maximum effective diffusion length is going to be shorter. Thus, as the organoid matures, the cells at the center of the bioprinted structure may be subject to necrosis because they are being starved of nutrients and can not remove their waste, while the cells at the edge will proliferate and expand. This flux of cell proliferation outwards and death inwards is the most likely cause of the variance at later time points. The IHC results (Fig. 4C–E) corroborate the proliferation study's results with increased KI67 and DAPI signal at the outer rim of the organoids. All IHC images can be seen in Supplemental Figs. 5 and 6, and 7.

If the growth was continued past the two-week study, it is projected to stabilize at some ATP value where the entire outer shell of the organoid is filled with cells. The signal could increase if the cells were laying down their own ECM to create a larger organoid. Currently, this poor diffusion is a limitation of this new bioink. However, as bioprinting hardware advances and printing resolution increases, this may be solved by simply generating internal channels in all bioprinted structures. Alternatively, we are currently assessing ways to maintain the beneficial mechanical properties of this bioink, while decreasing GNP concentration, thus potentially increasing diffusion properties internally.

Another reason for the overall variance is due to the distribution of organoid sizes. The data presented in Fig. 4A and B was all normalized to the mass of each organoid before being averaged to compensate for

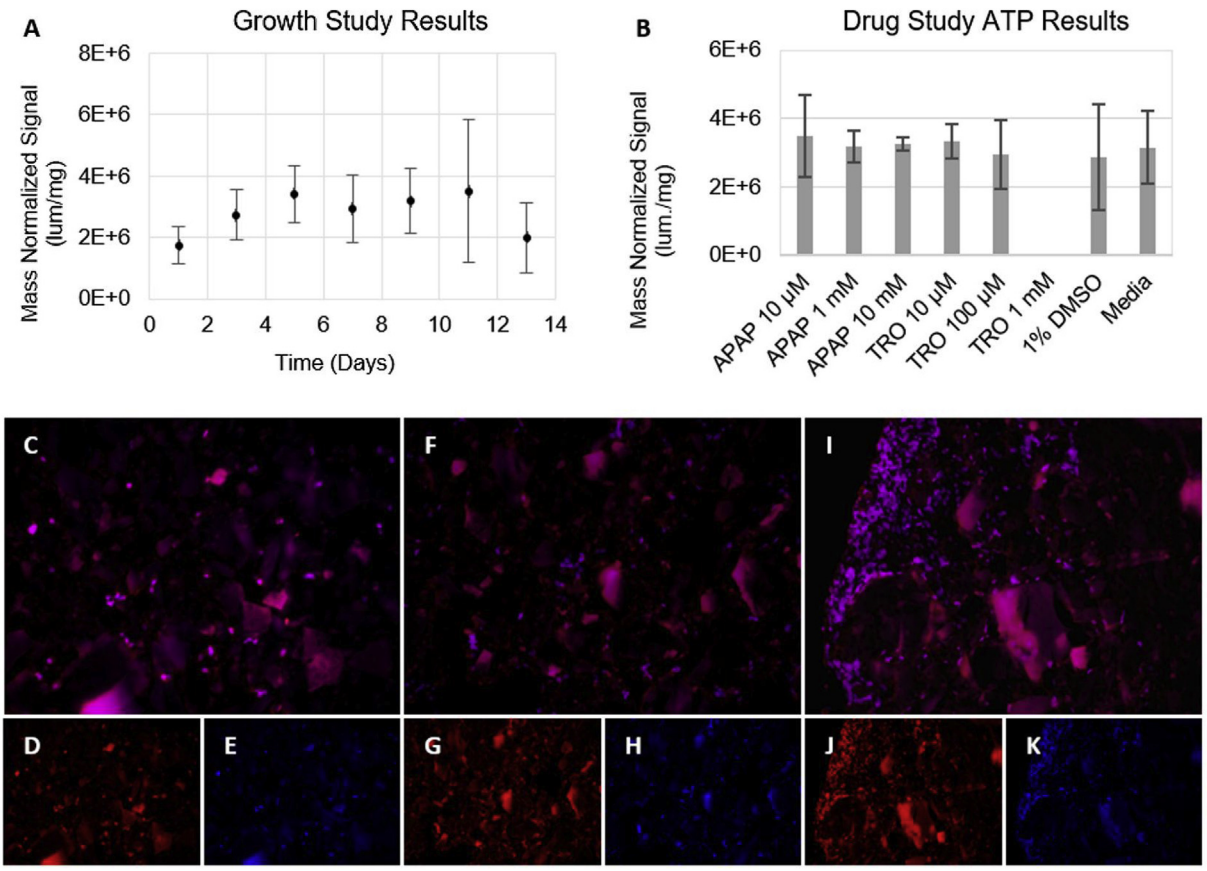

Fig. 4. A) Mass normalized ATP signal of organoids made with the GNP bioink and 5 M/mL HepG2 cells cultured 1–13 days, with a reading every other day. n = 6 per time point. **B)** Mass normalized ATP signal of organoids made with the GNP bioink and 5 M/mL HepG2 cells cultured for 7 days, then 2 days with media supplemented with the labeled drug, and then analyzed. IHC staining of organoids at C), D), E) day 1; **F), G), H)** day 7; and **I), J), K)** day 13 showing the HepG2 proliferation. Red is KI67, and blue is DAPI. (For interpretation of the references to color in this figure legend, the reader is referred to the Web version of this article.)

organoid sizes. The pneumatic bioprinter used for organoid printing applies a constant pressure to the bioink. At constant pressure thin bioink portions extrude fast, producing large organoids, and thick bioink portions extrude slowly, producing smaller organoids. To mitigate that issue, the pressure was adjusted on the fly, between 150 kPa and 300 kPa, to produce more consistent organoids. This helped with the printing procedure but did not entirely fix the variability. Assuming that the cells were mixed homogeneously into the bioink, the smaller organoids would produce a smaller ATP signal compared to the larger organoids. This does not mean that the smaller organoids are less viable, but rather that there are fewer total numbers of cells present. Biocompatibility is an intrinsic property between the material and the cells, and so it does not depend on organoid size. To compensate for larger organoids producing a larger signal, without any increase in intrinsic biocompatibility, the signal was normalized to organoid mass. This improved the quantification, but is an admittedly tedious process that is not realistically scalable.

An improved method would be to normalize to the shell volume of the organoid, which is approximately equal to the surface area of the organoid times the max diffusion length of oxygen and nutrients in the media. This would be the viable volume of the organoid. If the signals were normalized to this value, then only variance in cell density would affect the ATP signal. However, this would have been much more difficult to do since the organoids were not perfect spheres, nor did they have smooth surfaces. The mass of each organoid was used as an approximation of this. Another way of decreasing variance is by using the syringe pump printhead to precisely control the extruded volume. Then, all organoids would be very nearly the same size and mass, negating the need for any normalization. Currently, software limitations prevent the use of the syringe pump printhead with this immersion printing method.

Aside from proliferation, the organoids also behaved as expected when challenged with different drugs. Fig. 4B, on the right, shows the results from the drug study. The APAP did not significantly harm the HepG2 cells, and the TRO reached a critical value between 100 µM and 1 mM where it became toxic. The acetaminophen was not expected to damage the HepG2 cells because this cell line does not metabolize acetaminophen at the same rate as other hepatic cell lines, preventing the buildup of the toxic metabolite [36–38]. The troglitazone response was as expected with significant toxicity at 1 mM. Toxic effects are commonly reported above 100 µM [39,40].

4. Conclusion

The majority of current biologically-derived extrusion bioinks are not capable of creating self-supporting structures under ambient conditions without sacrificial support materials. However, the novel GNP-collagen-HA bioink described here is able to do just that. This bioink is comprised entirely of biological materials, all of which naturally occur within human tissue ECM. Successful harnessing of thixotropic mechanical properties enables this bioink to be mechanically stable and still be printable with fair precision. As bioprinter hardware and software continue to improve, this bioink will also have improved precision and capabilities. We also demonstrate that this bioink is capable of supporting cell growth, as shown by a growth study with HepG2 cells. GNPs have been widely used as drug and growth factor delivery vehicles, and incorporating GNPs loaded with growth factors or solubilized extra cellular matrix would further improve biocompatibility while retaining the robust mechanical properties. This bioink meets all the criteria of a successful extrusion bioink and will be employed in future more nuanced

bioprinting efforts to create viable tissue constructs for therapeutic and diagnostic applications.

Competing interests

The authors have no conflicts of interest to disclose.

Acknowledgements

The authors would like to acknowledge KyungMin Yoo and Hema Sivakumar for their contribution to this work. The authors acknowledge funding from the Medical Technology Enterprise Consortium under Contract # W81XWH-15-9-0001. The views and conclusions contained herein are those of the authors and should not be interpreted as necessarily representing the official policies or endorsements, either expressed or implied of the U.S. Government. The authors also acknowledge funding from the Wake Forest Baptist Medical Center Clinical and Translational Science Institute Open Pilot Program via NIH CTSA UL1 TR001420.

Appendix A. Supplementary data

Supplementary data to this article can be found online at https://doi.org/10.1016/j.bprint.2019.e00058.

References

[1] S.V. Murphy, A. Atala, 3D bioprinting of tissues and organs, Nat. Biotechnol. 32 (8) (Aug 2014) 773–785.
[2] I. Donderwinkel, J.C.M. van Hest, N.R. Cameron, Bio-inks for 3D bioprinting: recent advances and future prospects, Polym. Chem. 8 (31) (2017) 4451–4471, 10.1039/C7PY00826K.
[3] W. Peng, D. Unutmaz, I.T. Ozbolat, Bioprinting towards physiologically relevant tissue models for pharmaceutics, Trends Biotechnol. 34 (9) (Sep 2016) 722–732.
[4] S.H. Park, C.S. Jung, B.H. Min, Advances in three-dimensional bioprinting for hard tissue engineering, Tissue Eng. Regenerat. Med. 13 (6) (Dec 2016) 622–635.
[5] T. Billiet, M. Vandenhaute, J. Schelfhout, S. Van Vlierberghe, P. Dubruel, A review of trends and limitations in hydrogel-rapid prototyping for tissue engineering, Biomaterials 33 (26) (Sep 2012) 6020–6041.
[6] L.E. Bertassoni, et al., Hydrogel bioprinted microchannel networks for vascularization of tissue engineering constructs, Lab Chip 14 (13) (Jul 7 2014) 2202–2211.
[7] T. Boland, et al., Drop-on-demand printing of cells and materials for designer tissue constructs, Mater. Sci. Eng. C 27 (3) (2007/04/01/2007) 372–376.
[8] K. Christensen, C. Xu, W. Chai, Z. Zhang, J. Fu, Y. Huang, Freeform inkjet printing of cellular structures with bifurcations, Biotechnol. Bioeng. 112 (5) (May 2015) 1047–1055.
[9] Q. Gao, Y. He, J.Z. Fu, A. Liu, L. Ma, Coaxial nozzle-assisted 3D bioprinting with built-in microchannels for nutrients delivery, Biomaterials 61 (Aug 2015) 203–215.
[10] T.J. Hinton, et al., Three-dimensional printing of complex biological structures by freeform reversible embedding of suspended hydrogels, Sci. Adv. 1 (9) (2015), e1500758.
[11] A. Isaacson, S. Swioklo, C.J. Connon, 3D bioprinting of a corneal stroma equivalent, Exp. Eye Res. 173 (Aug 2018) 188–193.
[12] J. Jang, et al., 3D printed complex tissue construct using stem cell-laden decellularized extracellular matrix bioinks for cardiac repair, Biomaterials 112 (Jan 2017) 264–274.
[13] D.B. Kolesky, R.L. Truby, A.S. Gladman, T.A. Busbee, K.A. Homan, J.A. Lewis, 3D bioprinting of vascularized, heterogeneous cell-laden tissue constructs, Adv. Mater. 26 (19) (May 21 2014) 3124–3130.
[14] J.S. Miller, et al., Rapid casting of patterned vascular networks for perfusable engineered three-dimensional tissues, Nat. Mater. 11 (9) (Sep 2012) 768–774.
[15] C.M. Owens, F. Marga, G. Forgacs, C.M. Heesch, Biofabrication and testing of a fully cellular nerve graft, Biofabrication 5 (4) (Dec 2013), 045007.
[16] F. Pati, et al., Printing three-dimensional tissue analogues with decellularized extracellular matrix bioink, Nat. Commun. 5 (Jun 2 2014) 3935.
[17] W. Schuurman, et al., Gelatin-methacrylamide hydrogels as potential biomaterials for fabrication of tissue-engineered cartilage constructs, Macromol. Biosci. 13 (5) (May 2013) 551–561.
[18] X. Zhao, et al., In vitro vascularization of a combined system based on a 3D printing technique, J. Tissue Eng. Regenerat. Med. 10 (10) (Oct 2016) 833–842.
[19] K. Markstedt, A. Mantas, I. Tournier, H. Martinez Avila, D. Hagg, P. Gatenholm, 3D bioprinting human chondrocytes with nanocellulose-alginate bioink for cartilage tissue engineering applications, Biomacromolecules 16 (5) (May 11 2015) 1489–1496.
[20] R. Suntornnond, E.Y.S. Tan, J. An, C.K. Chua, A highly printable and biocompatible hydrogel composite for direct printing of soft and perfusable vasculature-like structures, Sci. Rep. 7 (1) (Dec 4 2017), 16902.
[21] A.J. Engler, S. Sen, H.L. Sweeney, D.E. Discher, Matrix elasticity directs stem cell lineage specification, Cell 126 (4) (Aug 25 2006) 677–689.
[22] D.E. Ingber, Cellular mechanotransduction: putting all the pieces together again, FASEB J. 20 (7) (May 2006) 811–827.
[23] J. Lopez-Barneo, J.R. Lopez-Lopez, J. Urena, C. Gonzalez, Chemotransduction in the carotid body: K+ current modulated by PO2 in type I chemoreceptor cells, Science 241 (4865) (1988) 580.
[24] R.J. Montoro, J. Ureña, R. Fernández-Chacón, G. Alvarez de Toledo, J. López-Barneo, Oxygen sensing by ion channels and chemotransduction in single glomus cells, J. Gen. Physiol. 107 (1) (1996) 133–143 (in eng).
[25] N. Wang, Review of cellular mechanotransduction, J. Phys. D Appl. Phys. 50 (23) (2017).
[26] R.G. Wells, The role of matrix stiffness in regulating cell behavior, Hepatology 47 (4) (Apr 2008) 1394–1400.
[27] G.D. Prestwich, Simplifying the extracellular matrix for 3-D cell culture and tissue engineering: a pragmatic approach, J. Cell. Biochem. 101 (6) (Aug 15 2007) 1370–1383.
[28] A. Skardal, J.M. Russo, P.V. Messina (Eds.), Biopolymers for Medical Applications, CRC Press, 2016.
[29] A. Skardal, Perspective: "Universal" bioink technology for advancing extrusion bioprinting-based biomanufacturing, Bioprinting 10 (2018).
[30] R. Chang, J. Nam, W. Sun, Effects of dispensing pressure and nozzle diameter on cell survival from solid freeform fabrication-based direct cell writing, Tissue Eng. A 14 (1) (Jan 2008) 41–48.
[31] K. Nair, et al., Characterization of cell viability during bioprinting processes, Biotechnol. J. 4 (8) (Aug 2009) 1168–1177.
[32] C.M. Smith, et al., Three-Dimensional BioAssembly tool for generating viable tissue-engineered constructs, Tissue Eng. 10 (9–10) (2004) 1566–1576, 2004/09/01.
[33] J. Mewis, N.J. Wagner, Thixotropy, Adv. Colloid Interface Sci. 147–148 (Mar-Jun 2009) 214–227.
[34] A. Mazzocchi, M. Devarasetty, R. Huntwork, S. Soker, A. Skardal, Optimization of collagen type I-hyaluronan hybrid bioink for 3D bioprinted liver microenvironments, Biofabrication 11 (1) (Oct 30 2018), 015003.
[35] K. L, H. VB, J. K, C.J. Coester, Gelatin nanoparticles by two step desolvation a new preparation method, surface modifications and cell uptake, J. Microencapsul. 17 (2) (2000) 187–193, 2000/01/01.
[36] N.J. Hewitt, P. Hewitt, Phase I and II enzyme characterization of two sources of HepG2 cell lines, Xenobiotica 34 (3) (2004) 243–256, 2004/03/01.
[37] C. Rodríguez-Antona, et al., Cytochrome P450 expression in human hepatocytes and hepatoma cell lines: molecular mechanisms that determine lower expression in cultured cells, Xenobiotica 32 (6) (2002) 505–520, 2002/01/01.
[38] S. Wilkening, F. Stahl, A. Bader, Comparison of primary human hepatocytes and hepatoma cell line HepG2 with regard to their biotransformation properties, Drug Metab. Dispos. 31 (8) (2003) 1035.
[39] D. Bavli, et al., Real-time monitoring of metabolic function in liver-on-chip microdevices tracks the dynamics of mitochondrial dysfunction, Proc. Natl. Acad. Sci. U. S. A. 113 (16) (Apr 19 2016) E2231–E2240.
[40] S.C. Ramaiahgari, et al., A 3D in vitro model of differentiated HepG2 cell spheroids with improved liver-like properties for repeated dose high-throughput toxicity studies, Arch. Toxicol. 88 (5) (May 2014) 1083–1095.